Fragmentation of positronium

C. Starrett,[1] Mary T. McAlinden,[2] and H. R. J. Walters[1]
[1]*Department of Applied Mathematics and Theoretical Physics, Queen's University, Belfast BT7 1NN, United Kingdom*
[2]*School of Computing and Mathematical Sciences, Oxford Brookes University, Wheatley Campus, Oxford OX33 1HX, United Kingdom*
(Received 28 February 2005; published 12 July 2005)

The impulse approximation is used to calculate cross sections for fragmentation of Ps($1s$) in collision with He, Ne, Ar, Kr, and Xe. Triple, double, single, and total cross sections are evaluated. Reasonably good agreement is found with the measurements of Armitage *et al.* [Phys. Rev. Lett. **89**, 173402 (2002)] on Ps($1s$)+He(1^1S) scattering. These absolute measurements comprise the total Ps ionization cross section and the cross section differential with respect to the longitudinal energy of the ejected positron. Characteristics of free electron and free positron scattering are explored in the double and triple differential cross sections for Ps($1s$)+Xe scattering.

DOI: 10.1103/PhysRevA.72.012508 PACS number(s): 36.10.Dr

I. INTRODUCTION

In a paper published in 2001 Ludlow and Walters [1] put forward some ideas on coincidence studies of positronium (Ps) fragmentation. In its most rigorous form the kinematics of such a study would be fully determined, i.e., one would measure the momentum of the incoming Ps, the momenta of the outgoing electron and positron, and one would have information on the initial and final states of the atomic target. The result of such an experiment would be a triple differential cross section (TDCS). In analogy with $(e,2e)$, Ludlow and Walters termed this a (Ps, e^+e^-) measurement. Their interest focused upon the idea that Ps, being a composite of a positron and an electron, might exhibit in its scattering some coherent combination of free electron and free positron scattering. In particular, if these two scatterings were sufficiently different in behavior, it might be possible, depending on the collision geometry, to see their "foot prints" in the Ps scattering. For example, we show in Fig. 1 differential cross sections for elastic $e^{\pm}-$Xe scattering in the static and static-exchange approximations. Whereas the positron cross sections are monotonically smooth, the electron cross sections, in the energy range shown, are highly structured. Such radical differences depend upon Xe being a many-electron atom with a well-developed shell structure, it would not be so for a light atom like He. Consequently, Ludlow and Walters recommended experiments on heavy targets such as Xe rather than light targets such as He.

The ideas of Ludlow and Walters are nicely encapsulated within the context of the impulse approximation (IA) [2,3] which treats the scattering of a composite, such as Ps, as a coherent sum of the individual scatterings of its constituents. The IA used here derives from that of Hartley and Walters [4–6] but with an interesting difference. Hartley and Walters studied collisions in which the projectile was a one-electron atom or ion. In their model the scattering of the projectile nucleus by the target was neglected, only the projectile electron scattered. The only function of the projectile nucleus was to interact with its electron giving it a distribution of momenta relative to the nucleus. By contrast, in the case of Ps as a projectile we must take account of the scattering of both particles, the electron and the positron, and combine these scatterings coherently. Ps scattering therfore provides an interesting window on this coherence property of the IA, a view not given by atom or ion projectiles.

Despite enormous advances in the experimental study of Ps-atom collisions [7–12], it will be some time before it is possible to measure a TDCS. However, the first measurement

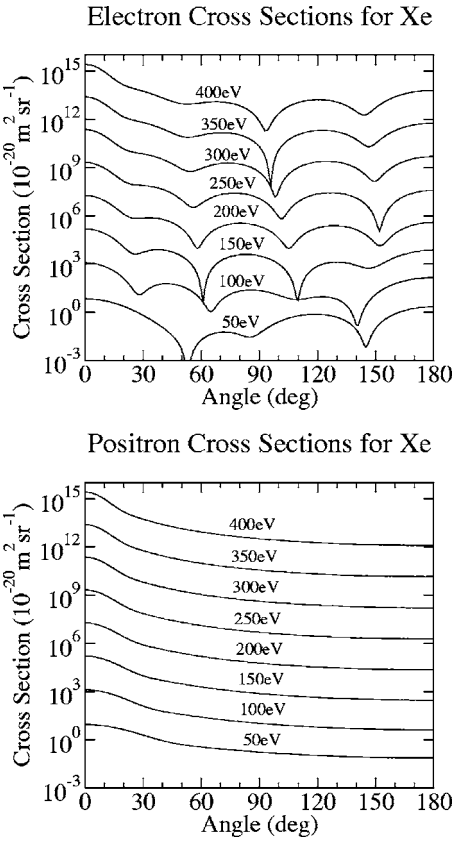

FIG. 1. Elastic differential cross sections for electron and positron scattering by Xe in the static-exchange and static approximations, respectively. The impact energy is indicated on each curve and the curves have been staggered by a factor of 10^2 on increasing the energy from 50 eV.

of a single differential cross section (SDCS) has recently been made [11,12], in this case the cross section differential with respect to the longitudinal energy of the ejected positron. Presently, therefore, there is a need to also look at less differential cross sections. Of course with each loss of differentiability we loose insight into the ionization mechanism and the coherent interplay between the electron and positron scatterings. The existing measurements [11,12] have been made on a He target and at relatively low impact energies ($\leqslant$33 eV). At impact energies below 27 eV excitation or ionization of the He is not possible and between 27 and 33 eV it should be unimportant [13,14], consequently we need only concentrate upon collisions in which the atom remains unexcited [15]. Although these energies are rather low for the IA, we believe that there is merit in applying it to the experimental data. The only other theoretical calculation of which we are aware is the classical trajectory Monte Carlo (CTMC) approximation of Sarkadi [16]. This compares well with the general pattern of the experimental data but gives cross sections of somewhat larger magnitude, furthermore, the exact details of the pattern are dependent upon the assumed range of the $e^{\pm}-$He interactions. A comparison with a different calculation, and in particular a quantal calculation, such as the IA, would therefore be appropriate. However, we do not restrict ourselves to He, nor to the energy range $\leqslant$33 eV. We look also, as recomended by Ludlow and Walters, towards the other end of the atomic scale, i.e., Xe, and at higher impact energies, up to 500 eV, where the validity of the IA improves. At high impact energies excitation of the target cannot be ignored [13]. Nevertheless, we shall restrict ourselves to target elastic collisions with the purpose of consolidating this part of the overall picture. The treatment of target inelastic collisions will require sums over final states, both bound and continuum, and a generally different approach [4–6,13,17], we leave this to a future publication.

The plan of the paper is as follows. In Sec. II we define and discuss the cross sections of interest: triple (TDCS); double (DDCS); single (SDCS); single differential with respect to the longitudinal energy of the ejected positron or electron (SDCSLP or SDCSLE); total (ionization). In Sec. III we discuss the first Born approximation (FBA) and, from it, develop the IA. In Sec. IV we give some calculational details and in Sec. V we present the results for target elastic collisions. Here we work "backwards," starting with the total ionization cross section and comparing the IA with experimental data on He [11,12] and with low energy ($\leqslant$40 eV) coupled pseudostate calculations on He, Ne, and Ar [14,18], this should give us some feeling for the overall validity of the approximation at those energies, although low, at which comparison is possible. For future reference, we also give the total ionization cross sections for Kr and Xe. Next we look at the longitudinal cross sections SDCSLP and SDCSLE, making comparison with the experimental results on He [11,12] and presenting predictions for Xe at the other end of the mass scale. Now confining ourselves to the two extremes, He and Xe, we work backwards through DDCSs and TDCSs, for which presently there are no experimental data, highlighting points of interest and general trends rather than giving exhaustive detail. In Sec. VI we record our conclusions. Unless otherwise stated we use atomic units (a.u.) in which $\hbar = m_e = e = 1$.

II. CROSS SECTIONS

Consider Ps in the state ϕ_a incident with velocity $\boldsymbol{v}_0$ upon an atomic target in the state ψ_b. If the Ps is ionized and the atom is left in the state $\psi_{b'}$ we can define the triple differential cross section (TDCS) $d^3\sigma_{bb'}/dEd\Omega_e\Omega_p$. This is the cross section for the positron (electron) appearing in a solid angle $d\Omega_p(d\Omega_e)$ about some specified direction while the energy of the positron or electron is in some specified range E to $E+dE$. From the TDCS we can generate by integration over $d\Omega_e, d\Omega_p$, or dE the double differential cross sections (DDCS):

$$\frac{d^2\sigma_{bb'}}{dEd\Omega_p}; \tag{1a}$$

$$\frac{d^2\sigma_{bb'}}{dEd\Omega_e}; \tag{1b}$$

$$\frac{d^2\sigma_{bb'}}{d\Omega_e d\Omega_p}. \tag{1c}$$

Further integration leads to the single differential cross sections (SDCS):

$$\frac{d\sigma_{bb'}}{dE}; \tag{2a}$$

$$\frac{d\sigma_{bb'}}{d\Omega_p}; \tag{2b}$$

$$\frac{d\sigma_{bb'}}{d\Omega_e}; \tag{2c}$$

and one more integration of Eqs. (2a)–(2c) gives the total Ps ionization cross section for a collision in which the atom goes from ψ_b to $\psi_{b'}$:

$$\sigma_{bb'}^{ion} = \int \frac{d^3\sigma_{bb'}}{dEd\Omega_e d\Omega_p} dE\Omega_e d\Omega_p. \tag{3}$$

In Refs. [11,12] it is the single differential cross section with respect to the longitudinal energy of the ejected positron that is measured. If the ejected positron has a velocity $\boldsymbol{v}_p$ making an angle θ_p with respect to the incident direction, then its longitudinal energy is

$$E_{pl} = \frac{1}{2}v_p^2 \cos^2\theta_p = E_p \cos^2\theta_p, \tag{4}$$

where $E_p = \frac{1}{2}v_p^2$ is its total energy. If the positron emerges in the forward cone, then

$$\frac{d\sigma_{bb'}^F}{dE_{pl}} = 2\pi \int_{\sqrt{E_{pl}/E_m}}^1 \frac{d^2\sigma_{bb'}}{dEd\Omega_p}\left(E_p = \frac{E_{pl}}{\cos^2\theta_p}, \cos\theta_p\right)\frac{d(\cos\theta_p)}{\cos^2\theta_p} \tag{5a}$$

$$= \frac{\pi}{\sqrt{E_{pl}}} \int_{E_{pl}}^{E_m} \frac{d^2\sigma_{bb'}}{dEd\Omega_p}\left(E_p, \cos\,\theta_p = \sqrt{\frac{E_{pl}}{E_p}}\right)\frac{dE_p}{\sqrt{E_p}}. \quad (5b)$$

If it emerges in the backward cone we get

$$\frac{d\sigma^B_{bb'}}{dE_{pl}} = 2\pi \int_{-1}^{-\sqrt{E_{pl}/E_m}} \frac{d^2\sigma_{bb'}}{dEd\Omega_p}\left(E_p = \frac{E_{pl}}{\cos^2\,\theta_p}, \cos\,\theta_p\right)\frac{d(\cos\,\theta_p)}{\cos^2\,\theta_p} \quad (6a)$$

$$= \frac{\pi}{\sqrt{E_{pl}}} \int_{E_{pl}}^{E_m} \frac{d^2\sigma_{bb'}}{dEd\Omega_p}\left(E_p, \cos\,\theta_p = -\sqrt{\frac{E_{pl}}{E_p}}\right)\frac{dE_p}{\sqrt{E_p}}. \quad (6b)$$

In Eqs. (5a), (5b), (6a), and (6b) we have assumed that the initial state of the Ps and the initial and final states of the atom are spherically symmetric so that $d^2\sigma_{bb'}/dEd\Omega_p$ is independant of the azimuthal angle ϕ_p of the ejected positron about the incident direction. We also indicate by $d^2\sigma_{bb'}(E_p, \cos\,\theta_p)/dEd\Omega_p$ the functional dependence of the DDCS on E_p and θ_p. The quantity E_m is the maximum possible energy of the emitted positron:

$$E_m = v_0^2 + \epsilon_b - \epsilon_{b'} - I_a^{\mathrm{Ps}}, \quad (7)$$

where ϵ_b is the energy of the atomic state ψ_b and I_a^{Ps} is the ionization potential of the Ps in the state ϕ_a.

In the experiment of [11,12] backward moving positrons are reflected forwards by a repulsive grid so that both backward and forward positrons are collected [19]. The appropriate cross section is then the sum of Eqs. 5 and 6, i.e.,

$$\frac{d\sigma_{bb'}}{dE_{pl}} = \frac{d\sigma^F_{bb'}}{dE_{pl}} + \frac{d\sigma^B_{bb'}}{dE_{pl}}. \quad (8)$$

It is this that we shall refer to as the single differential cross section with respect to the longitudinal energy of the ejected positron (SDCSLP).

From Eqs. (5b) and (6b) we see that the longitudinal cross section becomes infinite as $1/\sqrt{E_{pl}}$ as E_{pl} tends to zero. In this limit

$$\frac{d\sigma_{bb'}}{dE_{pl}} = 2\frac{d\sigma^F_{bb'}}{dE_{pl}} = 2\frac{d\sigma^B_{bb'}}{dE_{pl}} = \frac{C^p_{bb'}}{\sqrt{E_{pl}}}, \quad (9)$$

where the constant $C^p_{bb'}$ is given by

$$C^p_{bb'} = 2\pi \int_0^{E_m} \frac{d^2\sigma_{bb'}}{dEd\Omega_p}(E_p, \cos\,\theta_p = 0)\frac{dE_p}{\sqrt{E_p}}. \quad (10)$$

Analogously we can write down a cross section differential with respect to the longitudinal energy $E_{el} = \frac{1}{2}v_e^2\cos^2\,\theta_e$ of the ejected electron. Here we start from the DDCS $d^2\sigma_{bb'}/dEd\Omega_e$. The advantage of detecting the positron rather than the electron is that the source of the positron is unambigious, it must come from the Ps. The electron analog of Eq. (8) we label as SDCSLE.

Finally, we note that the ionization cross section $\sigma^{ion}_{bb'}$ decreases as $1/E_0$ as $E_0 \to \infty$, where $E_0 = v_0^2$ is the impact energy of the Ps, see Appendix B.

III. THEORY

We consider the scattering of Ps by an N-electron neutral atom. We denote by $\boldsymbol{r}_i (i=1,2,\ldots,N)$ the position vector of the ith target electron and by $\boldsymbol{r}_e$ and $\boldsymbol{r}_p$ the position vectors of the electron and positron forming the Ps. All position vectors are referred to the atomic nucleus as origin. The center of mass of the positronium is then given by $\boldsymbol{R} \equiv (\boldsymbol{r}_p + \boldsymbol{r}_e)/2$ and its internal coordinate by $\boldsymbol{t} \equiv \boldsymbol{r}_p - \boldsymbol{r}_e$. We take the Ps to be initially in the state $\phi_a(\boldsymbol{t})$ (energy E_a) and incident with velocity $\boldsymbol{v}_0$ upon the atom in a state $\psi_b(\boldsymbol{X})$ (energy ϵ_b). In the atom wave function $\boldsymbol{X}$ stands for the aggregate of the space and spin coordinates $\boldsymbol{x}_i \equiv (\boldsymbol{r}_i, s_i)$ of the atomic electrons i.e., $\boldsymbol{X} \equiv (\boldsymbol{x}_1, \boldsymbol{x}_2, \ldots, \boldsymbol{x}_N)$. We begin in Sec. III A by looking at the first Born approximation for the collision. By interpreting the first Born approximation we then give an intuitive development of the impulse approximation in Sec. III B.

A. The first Born approximation (FBA)

If the collision of the Ps with the atom results in a change of state of the Ps from ϕ_a to $\phi_{a'}$, while the atom changes state from ψ_b to $\psi_{b'}$, then the FBA amplitude for this process is given by

$$f^{B1}(\mathrm{Ps}{:}a \to a'; \mathrm{atom}{:}b \to b') = -\frac{1}{\pi}\left\langle e^{i\boldsymbol{p}_f\cdot\boldsymbol{R}}\phi_{a'}(\boldsymbol{t})\psi_{b'}(\boldsymbol{X}) \times |V| e^{i\boldsymbol{p}_0\cdot\boldsymbol{R}}\phi_a(\boldsymbol{t})\psi_b(\boldsymbol{X})\right\rangle, \quad (11)$$

where $\boldsymbol{p}_0 = 2\boldsymbol{v}_0$ ($\boldsymbol{p}_f = 2\boldsymbol{v}_f$) is the initial (final) momentum of the Ps relative to the atom and V is the interaction between the Ps and the atom,

$$V = \left(\sum_{i=1}^{N}\frac{1}{|\boldsymbol{r}_e - \boldsymbol{r}_i|} - \frac{Z}{r_e}\right) - \left(\sum_{i=1}^{N}\frac{1}{|\boldsymbol{r}_p - \boldsymbol{r}_i|} - \frac{Z}{r_p}\right). \quad (12)$$

In Eq. (12) $Z(=N)$ is the nuclear charge. Using Bethe's integral Eq. (11) may be written

$$f^{B1}(\mathrm{Ps}{:}a \to a'; \mathrm{atom}{:}b \to b') = 2\langle\phi_{a'}(\boldsymbol{t})|e^{-i\boldsymbol{q}\cdot\boldsymbol{t}/2}|\phi_a(\boldsymbol{t})\rangle f^{B1+}_{bb'}(\boldsymbol{q}) + 2\langle\phi_{a'}(\boldsymbol{t})|e^{i\boldsymbol{q}\cdot\boldsymbol{t}/2}|\phi_a(\boldsymbol{t})\rangle f^{B1-}_{bb'}(\boldsymbol{q}), \quad (13)$$

where

$$f^{B1\pm}_{bb'}(\boldsymbol{q}) = \pm\frac{2}{q^2}\langle\psi_{b'}(\boldsymbol{X})|\left(-Z + \sum_{i=1}^{N} e^{i\boldsymbol{q}\cdot\boldsymbol{r}_i}\right)|\psi_b(\boldsymbol{X})\rangle \quad (14)$$

and $\boldsymbol{q} = \boldsymbol{p}_0 - \boldsymbol{p}_f$ is the momentum transfer in the collision.

Formula (13) has an interesting structure. The quantities $f^{B1\pm}_{bb'}(\boldsymbol{q})$, as our notation implies, are identical to the FBA amplitudes for free positron (+) and free electron (−) scattering by the atom where $\boldsymbol{q}$ is the momentum transfer in the collision. Formula (13) may then be interpreted as a coherent combination of independent free scatterings of the electron and positron in the Ps, these scatterings being modified by a form factor, $\langle\phi_{a'}(\boldsymbol{t})|e^{\pm i\boldsymbol{q}\cdot\boldsymbol{t}/2}|\phi_a(\boldsymbol{t})\rangle$, which describes how the initial Ps state ϕ_a is transformed into the final Ps state ϕ'_a. It is this idea which motivates the impulse approximation of Sec. III B.

With the normalization (11) the differential cross section for the scattering is given by

$$\frac{d\sigma^{B1}}{d\Omega_{\rm Ps}} = \frac{v_f}{v_0}|f^{B1}|^2, \tag{15}$$

where $d\Omega_{\rm Ps}$ is the solid angle into which the center of mass of the Ps is scattered (the direction of $\boldsymbol{p}_f$) and where we have assumed that $\phi_{a'}$ and $\psi_{b'}$ are bound states. However, here we are interested in the case where the Ps is ionized although the atom remains bound. In this case $\phi_{a'}$ needs to be a continuum state of Ps with ingoing scattered wave boundary conditions, $\phi^-_{\boldsymbol{\kappa}}(\boldsymbol{t})$ say, where $\boldsymbol{\kappa}$ is the momentum of the positron relative to the electron, i.e.,

$$\boldsymbol{\kappa} = \frac{1}{2}(\boldsymbol{v}_p - \boldsymbol{v}_e), \tag{16}$$

$\boldsymbol{v}_p$ and $\boldsymbol{v}_e$ being the velocities of the ejected positron and electron and $1/2$ being the reduced mass of the Ps system. We therefore take $\phi_{a'}$ in Eq. (13) to be the Coulomb function

$$\phi^-_{\boldsymbol{\kappa}}(\boldsymbol{t}) = \frac{1}{(2\pi)^{3/2}}\exp\left(\frac{1}{2}\pi\nu\right)\Gamma(1+i\nu)e^{i\boldsymbol{\kappa}\cdot\boldsymbol{t}} \times {}_1F_1(-i\nu,1,-i(\kappa t + \boldsymbol{\kappa}\cdot\boldsymbol{t})) \tag{17}$$

$$\nu = \frac{1}{2\kappa}. \tag{18}$$

Generalizing Eq. (15) we can write

$$\frac{d^3\sigma^{B1}_{bb'}}{d\Omega_{\rm Ps}d\boldsymbol{\kappa}} = \frac{v_f}{v_0}|f^{B1}({\rm Ps}{:}a\to\boldsymbol{\kappa};{\rm atom}{:}b\to b')|^2, \tag{19}$$

where

$$f^{B1}({\rm Ps}{:}a\to\boldsymbol{\kappa};{\rm atom}{:}b\to b') = 2\langle\phi^-_{\boldsymbol{\kappa}}(\boldsymbol{t})|e^{-i\boldsymbol{q}\cdot\boldsymbol{t}/2}|\phi_a(\boldsymbol{t})\rangle f^{B1+}_{bb'}(\boldsymbol{q}) + 2\langle\phi^-_{\boldsymbol{\kappa}}(\boldsymbol{t})|e^{i\boldsymbol{q}\cdot\boldsymbol{t}/2}|\phi_a(\boldsymbol{t})\rangle f^{B1-}_{bb'}(\boldsymbol{q}) \tag{20}$$

and

$$\boldsymbol{v}_f = \frac{1}{2}(\boldsymbol{v}_p + \boldsymbol{v}_e). \tag{21}$$

What we need here, however, is the TDCS $d^3\sigma_{bb'}/dEd\Omega_e d\Omega_p$. In Appendix A we show that this TDCS is correspondingly

$$\frac{d^3\sigma^{B1}_{bb'}}{dEd\Omega_e d\Omega_p} = \frac{v_p v_e}{4v_0}|f^{B1}({\rm Ps}{:}a\to\boldsymbol{\kappa};{\rm atom}{:}b\to b')|^2. \tag{22}$$

From Eqs. (17) and (20) we see that a factor

$$\exp(\pi\nu)|\Gamma(1+i\nu)|^2 \tag{23}$$

must appear in the TDCS (22). In the limit $\kappa\to 0(\nu\to\infty)$ this factor diverges as $1/\kappa$ [23]. Thus the TDCS becomes infinite as $1/|\boldsymbol{v}_p-\boldsymbol{v}_e|$ as $\boldsymbol{v}_p\to\boldsymbol{v}_e$. This is the well-known electron loss to the continuum (ELC) cusp [24] which can be observed in electron loss from neutral atoms and positive ions. The ELC cusp is a feature of the TDCS in its own right, see formula (A7), it is not an artifact of the FBA.

The FBA is symmetrical between the electron and the positron, i.e., the electron and positron spectra are identical. This is easily seen from Eq. (20). If the velocities of the outgoing electron and positron are interchanged then $\boldsymbol{\kappa}\to-\boldsymbol{\kappa}$, see Eq. (16), while $\boldsymbol{q}=2\boldsymbol{v}_0-\boldsymbol{v}_p-\boldsymbol{v}_e$ remains unchanged. It is an easy matter to show that

$$\langle\phi^-_{-\boldsymbol{\kappa}}(\boldsymbol{t})|e^{\pm i\boldsymbol{q}\cdot\boldsymbol{t}/2}|\phi_a(\boldsymbol{t})\rangle = P_a\langle\phi^-_{\boldsymbol{\kappa}}(\boldsymbol{t})|e^{\mp i\boldsymbol{q}\cdot\boldsymbol{t}/2}|\phi_a(\boldsymbol{t})\rangle, \tag{24}$$

where P_a is the parity of the Ps state $\phi_a(\boldsymbol{t})$. Then, using the trivial fact that $f^{B1\pm}_{bb'}(\boldsymbol{q}) = -f^{B1\mp}_{bb'}(\boldsymbol{q})$, see Eq. (14), we see that the effect of the interchange is to convert f^{B1} into $-P_a f^{B1}$ which has no effect on the TDCS (22). In an obvious notation it follows that

$$\frac{d^3\sigma^{B1}_{bb'}}{dEd\Omega_e d\Omega_p}(\boldsymbol{v}_p=\boldsymbol{v},\boldsymbol{v}_e=\boldsymbol{v}') = \frac{d^3\sigma^{B1}_{bb'}}{dEd\Omega_e d\Omega_p}(\boldsymbol{v}_p=\boldsymbol{v}',\boldsymbol{v}_e=\boldsymbol{v}), \tag{25a}$$

$$\frac{d^2\sigma^{B1}_{bb'}}{dEd\Omega_p}(\boldsymbol{v}_p=\boldsymbol{v}) = \frac{d^2\sigma^{B1}_{bb'}}{dEd\Omega_e}(\boldsymbol{v}_e=\boldsymbol{v}), \tag{25b}$$

$$\frac{d^2\sigma^{B1}_{bb'}}{d\Omega_e d\Omega_p}(\hat{\boldsymbol{v}}_p=\hat{\boldsymbol{v}},\hat{\boldsymbol{v}}_e=\hat{\boldsymbol{v}}') = \frac{d^2\sigma^{B1}_{bb'}}{d\Omega_e d\Omega_p}(\hat{\boldsymbol{v}}_p=\hat{\boldsymbol{v}}',\hat{\boldsymbol{v}}_e=\hat{\boldsymbol{v}}), \tag{25c}$$

$$\frac{d\sigma^{B1}_{bb'}}{d\Omega_p}(\hat{\boldsymbol{v}}_p=\hat{\boldsymbol{v}}) = \frac{d\sigma^{B1}_{bb'}}{d\Omega_e}(\hat{\boldsymbol{v}}_e=\hat{\boldsymbol{v}}), \tag{25d}$$

$$\frac{d\sigma^{B1}_{bb'}}{dE}(v_p=v,v_e=v') = \frac{d\sigma^{B1}_{bb'}}{dE}(v_p=v',v_e=v), \tag{25e}$$

$$\frac{d\sigma^{B1}_{bb'}}{dE_{pl}}(E_{pl}=E_l) = \frac{d\sigma^{B1}_{bb'}}{dE_{pl}}(E_{el}=E_l), \tag{25f}$$

where a caret denotes a unit vector. The condition (25e) means that $d\sigma^{B1}_{bb'}/dE$ is symmetric in the ejected energy E about $E=\frac{1}{2}E_m$ where E_m is the maximum ejected energy defined in Eq. (7).

The FBA is appropriate when the interaction between the Ps and the atom is weak or when the impact energy is sufficiently high. Experience with electron, atom, and Ps collisions [4,6,13,25,26] with "heavy" atoms such as, e.g., Ar, Kr, and Xe, indicates that the FBA does not become viable until quite high impact energies for collisions in which the atom remains in its initial state (a "target elastic" process). The problem lies with the increasing static potential presented to the projectile by the atom as the atom grows in size. Here, we wish to be able to study collisions of Ps not only with He but with any atom. We seek therefore an approximation which will not be so susceptible to the growth in the static potential of the atom and will therefore be viable at much lower impact energies. The impulse approximation is such an approximation.

B. The impulse approximation (IA)

We begin with an interpretation of the FBA (13). We first introduce the relative momentum distribution function $g_\alpha(\boldsymbol{Q})$ for an arbitrary Ps state $\phi_\alpha(\boldsymbol{t})$:

$$g_\alpha(\boldsymbol{Q}) = \frac{1}{(2\pi)^{3/2}} \int e^{-i\boldsymbol{Q}\cdot\boldsymbol{t}} \phi_\alpha(\boldsymbol{t}) d\boldsymbol{t}. \tag{26}$$

Then Eq. (13) may be written

$$\begin{aligned} f^{B1}(\mathrm{Ps}:a \to a';\mathrm{atom}:b \to b') &= 2\left\{ \int g^*_{a'}(\boldsymbol{Q}'') \delta\left(\boldsymbol{Q}' - \boldsymbol{Q}'' - \frac{\boldsymbol{q}}{2}\right) \right. \\ &\times g_a(\boldsymbol{Q}') f^{B1+}_{bb'}(\boldsymbol{q}) d\boldsymbol{Q}' d\boldsymbol{Q}'' \\ &+ \int g^*_{a'}(\boldsymbol{Q}'') \delta\left(\boldsymbol{Q}' - \boldsymbol{Q}'' + \frac{\boldsymbol{q}}{2}\right) \\ &\left. \times g_a(\boldsymbol{Q}') f^{B1-}_{bb'}(\boldsymbol{q}) d\boldsymbol{Q}' d\boldsymbol{Q}'' \right\}. \end{aligned} \tag{27}$$

We think of the electron and the positron in the state $\phi_a(\boldsymbol{t})$ as having a distribution of velocities $\boldsymbol{v}'_p$ and $\boldsymbol{v}'_e$ where

$$\boldsymbol{Q}' = \frac{1}{2}(\boldsymbol{v}'_p - \boldsymbol{v}'_e). \tag{28}$$

If these velocities are measured relative to the target then, since the Ps center of mass is incident with velocity $\boldsymbol{v}_0$, we must also have

$$\boldsymbol{v}_0 = \frac{1}{2}(\boldsymbol{v}'_p + \boldsymbol{v}'_e). \tag{29}$$

Analogously, the final state $\phi_{a'}$ will have a distribution of velocities $\boldsymbol{v}''_p$ and $\boldsymbol{v}''_e$ with

$$\boldsymbol{Q}'' = \frac{1}{2}(\boldsymbol{v}''_p - \boldsymbol{v}''_e), \tag{30}$$

$$\boldsymbol{v}_f = \frac{1}{2}(\boldsymbol{v}''_p + \boldsymbol{v}''_e). \tag{31}$$

Consider the first term in Eq. (27). The delta function condition gives

$$\boldsymbol{Q}' = \boldsymbol{Q}'' + \frac{\boldsymbol{q}}{2}$$

$$\Rightarrow \boldsymbol{v}'_p - \boldsymbol{v}'_e = \boldsymbol{v}''_p - \boldsymbol{v}''_e + \boldsymbol{q}. \tag{32}$$

In this term only the positron scatters off the atom so we should have $\boldsymbol{v}''_e = \boldsymbol{v}'_e$ and so Eq. (32) reduces to

$$\boldsymbol{v}'_p - \boldsymbol{v}''_p = \boldsymbol{q}. \tag{33}$$

This is consistent with the argument of $f^{B1+}_{bb'}(\boldsymbol{q})$, i.e., the whole momentum transfer $\boldsymbol{q}$ of the Ps is borne by the positron in its collision with the target. An analogous interpretation applies to the second term in Eq. (27) but now it is the electron that carries the whole burden of the scattering. The overall scattering (27) is the coherent sum of these two independent collision routes.

The weakness of the FBA is its perturbative treatment of the $e^\pm$-target interactions, represented in Eq. (27) by the first order amplitudes $f^{B1\pm}_{bb'}(\boldsymbol{q})$. If these could be replaced by more realistic nonperturbative estimates then the approximation might be much more viable. Unlike the first Born amplitudes $f^{B1\pm}_{bb'}(\boldsymbol{q})$ more realistic treatments of free electron/positron scattering by the target would not depend only upon the momentum transfer $\boldsymbol{q}$, they would, in general, depend upon the initial and final velocities of the scattering electron/positron, i.e., upon $\boldsymbol{v}'_e$ and $\boldsymbol{v}''_e$, $\boldsymbol{v}'_p$ and $\boldsymbol{v}''_p$. Making such a replacement we therefore write Eq. (27) as

$$\begin{aligned} f^{IA}(\mathrm{Ps}:a \to a';\mathrm{atom}:b \to b') &= 2\left\{ \int g^*_{a'}(\boldsymbol{Q}'') \delta\left(\boldsymbol{Q}' - \boldsymbol{Q}'' - \frac{\boldsymbol{q}}{2}\right) \right. \\ &\times g_a(\boldsymbol{Q}') f^{+}_{bb'}(\boldsymbol{v}'_p, \boldsymbol{v}''_p) d\boldsymbol{Q}' d\boldsymbol{Q}'' \\ &+ \int g^*_{a'}(\boldsymbol{Q}'') \delta\left(\boldsymbol{Q}' - \boldsymbol{Q}'' + \frac{\boldsymbol{q}}{2}\right) \\ &\left. \times g_a(\boldsymbol{Q}') f^{-}_{bb'}(\boldsymbol{v}'_e, \boldsymbol{v}''_e) d\boldsymbol{Q}' d\boldsymbol{Q}'' \right\}, \end{aligned} \tag{34}$$

where the velocities $\boldsymbol{v}'_p, \boldsymbol{v}''_p, \boldsymbol{v}'_e$, and $\boldsymbol{v}''_e$ are defined as functions of $\boldsymbol{Q}'$ and $\boldsymbol{Q}''$ by [see Eqs. (28)–(31)]

$$\boldsymbol{v}'_p = \boldsymbol{v}_0 + \boldsymbol{Q}', \tag{35a}$$

$$\boldsymbol{v}'_e = \boldsymbol{v}_0 - \boldsymbol{Q}', \tag{35b}$$

$$\boldsymbol{v}''_p = \boldsymbol{v}_f + \boldsymbol{Q}'' = \boldsymbol{v}_0 + \boldsymbol{Q}'' - \frac{\boldsymbol{q}}{2}, \tag{35c}$$

$$\boldsymbol{v}''_e = \boldsymbol{v}_f - \boldsymbol{Q}'' = \boldsymbol{v}_0 - \boldsymbol{Q}'' - \frac{\boldsymbol{q}}{2}. \tag{35d}$$

Formula (34) defines the impulse approximation.

Although the IA relaxes the assumption that the interaction between the projectile and target is weak, it is still in essence a "high energy" approximation. The approximation implies that the constituents of the projectile scatter indpendently, this requires that the impact energy be not too low. Roughly speaking, the impact energy should be "large" compared with the binding energy of the projectile. We note that the binding energy of Ps($1s$) is 6.8 eV.

There is a problem with Eq. (34), the amplitudes $f^{\pm}_{bb'}(\boldsymbol{v}', \boldsymbol{v}'')$ are not fully defined. The difficulty is that, in general, the velocities will be off-energy-shell [see Eqs. (35a)–(35d)], i.e.,

$$\frac{v'^2}{2} + \epsilon_b \neq \frac{v''^2}{2} + \epsilon_{b'}. \tag{36}$$

Ignoring any exchange effects we can write [27]

$$f^{\pm}_{bb'}(\boldsymbol{v}',\boldsymbol{v}'') = -\frac{1}{2\pi}\langle e^{i\boldsymbol{v}''\cdot\boldsymbol{r}}\psi_{b'}(\boldsymbol{X})|$$
$$[V + V(E + i\eta - H)^{-1}V]|e^{i\boldsymbol{v}'\cdot\boldsymbol{r}}\psi_b(\boldsymbol{X})\rangle. \quad (37)$$

Here V is the $e^{\pm}$-target interaction, H is the full Hamiltonian for the $e^{\pm}$ colliding with the target, and $\eta\to 0+$. For real physical scattering

$$E = \frac{v'^2}{2} + \epsilon_b = \frac{v''^2}{2} + \epsilon'_b. \quad (38)$$

While $\boldsymbol{v}'$ and $\boldsymbol{v}''$ are given in Eqs. (35a)–(35d), E is not defined because of the inequality (36). What then should E be? There is no definite answer to this question. The ambiguity in what to take for E reflects the basic inconsistency of the IA, namely, that bound particles are treated as if they were free. Following Hartley and Walters [5] we therefore opt for a reasonable and convenient prescription that seems to have worked well for atom and ion projectiles [5,6].

In the situation of interest here $b'=b$ so that we are concerned with the elastic scattering off the target, let us write $f^{\pm}_{bb}=f^{\pm}_{el}$. The suggestion of Hartley and Walters is to take $f^{\pm}_{el}$ to be the physical on-energy-shell scattering amplitude. Since our chosen targets are all spherically symmetric $f^{\pm}_{el}$ will be a function only of the impact speed, $\bar{v}$ say, and the magnitude of the momentum transfer $\boldsymbol{q}$. Hartley and Walters give the prescription

$$f^{\pm}_{bb}(\boldsymbol{v}',\boldsymbol{v}'') \to f^{\pm}_{el}(\bar{v},q), \quad (39a)$$

$$\boldsymbol{q} = \boldsymbol{v}' - \boldsymbol{v}'', \quad (39b)$$

$$\bar{v} = \mathrm{Max}(v',v''), \quad (39c)$$

where $\mathrm{Max}(v',v'')$ means the greater of v' and v''. The choice (39c) guarantees that $0\leqslant q\leqslant 2\bar{v}$, a necessary condition for physical on-energy-shell elastic scattering. Using the prescription (39a)–(39c) in Eq. (34) we get as our IA for target elastic collisions

$$f^{IA}(\mathrm{Ps}{:}a\to a';\mathrm{atom}{:}b\to b) = 2\left\{\int g^{*}_{a'}(\boldsymbol{Q}'')\,\delta\left(\boldsymbol{Q}' - \boldsymbol{Q}'' - \frac{\boldsymbol{q}}{2}\right) \times g_a(\boldsymbol{Q}')f^{+}_{el}(\bar{v}^{+},q)\,d\boldsymbol{Q}'\,d\boldsymbol{Q}'' + \int g^{*}_{a'}(\boldsymbol{Q}'')\,\delta\left(\boldsymbol{Q}' - \boldsymbol{Q}'' + \frac{\boldsymbol{q}}{2}\right) \times g_a(\boldsymbol{Q}')f^{-}_{el}(\bar{v}^{-},q)\,d\boldsymbol{Q}'\,d\boldsymbol{Q}''\right\} \quad (40a)$$

$$\bar{v}^{\pm} = \mathrm{Max}\left(|\boldsymbol{v}_0 \pm \boldsymbol{Q}'|, \left|\boldsymbol{v}_0 \pm \boldsymbol{Q}'' - \frac{\boldsymbol{q}}{2}\right|\right). \quad (40b)$$

The approximation (40a) and (40b) requires a nontrivial three-dimensional integration over $\boldsymbol{Q}'$ or $\boldsymbol{Q}''$. Again following Hartley and Walters [5] we simplify matters by invoking a peaking approximation which is a further assumption over and above the impulse approximation. If we assume that $g_{a'}(\boldsymbol{Q}'')$ is peaked at $\boldsymbol{Q}''=\boldsymbol{c}$, say, and that the scattering amplitudes are slowly varying in the vicinity of this point, then it should be a resonable approximation to evaluate the $f^{\pm}_{el}$ at $\boldsymbol{Q}''=\boldsymbol{c}$ and remove them to outside the integrals. The remaining integrals are then recognized as originating from the form factors in Eq. (13). With this peaking assumption the IA (40a) and (40b) reduces to

$$f^{IA,\mathrm{Peak}}(\mathrm{Ps}{:}a\to a';\mathrm{atom}{:}b\to b) = 2\langle\phi_{a'}(\boldsymbol{t})|e^{-i\boldsymbol{q}\cdot\boldsymbol{t}/2}|\phi_a(\boldsymbol{t})\rangle f^{+}_{el}(\bar{v}^{+},q) + 2\langle\phi_{a'}(\boldsymbol{t})|e^{i\boldsymbol{q}\cdot\boldsymbol{t}/2}|\phi_a(\boldsymbol{t})\rangle f^{-}_{el}(\bar{v}^{-},q), \quad (41a)$$

$$\bar{v}^{\pm} = \mathrm{Max}\left(\left|\boldsymbol{v}_0 \pm \boldsymbol{c} + \frac{\boldsymbol{q}}{2}\right|, \left|\boldsymbol{v}_0 \pm \boldsymbol{c} - \frac{\boldsymbol{q}}{2}\right|\right). \quad (41b)$$

In Eq. (41a) we have returned to the FBA formula (13) but with the first Born $e^{\pm}$-target amplitudes now replaced by the more realistic estimates $f^{\pm}_{el}$.

The peaking approximation is particularly appropriate to the present context where $\phi_{a'}$ is the continuum state $\phi^{-}_{\boldsymbol{\kappa}}$. For such a state $g_{a'}(\boldsymbol{Q}'')$ should have a peak, in fact a delta function like behavior [28], at $\boldsymbol{Q}''=\boldsymbol{\kappa}$. The approximation (41a) and (41b) for target elastic collisions then becomes

$$f^{IA,\mathrm{Peak}}(\mathrm{Ps}{:}a\to\boldsymbol{\kappa};\mathrm{atom}{:}b\to b) = 2\langle\phi^{-}_{\boldsymbol{\kappa}}(\boldsymbol{t})|e^{-i\boldsymbol{q}\cdot\boldsymbol{t}/2}|\phi_a(\boldsymbol{t})\rangle f^{+}_{el}(\bar{v}^{+},q) + 2\langle\phi^{-}_{\boldsymbol{\kappa}}(\boldsymbol{t})|e^{i\boldsymbol{q}\cdot\boldsymbol{t}/2}|\phi_a(\boldsymbol{t})\rangle f^{-}_{el}(\bar{v}^{-},q), \quad (42a)$$

where, from Eqs. (16) and (21) and $\boldsymbol{q}=2(\boldsymbol{v}_0-\boldsymbol{v}_f)$,

$$\boldsymbol{\kappa} = \frac{1}{2}(\boldsymbol{v}_p - \boldsymbol{v}_e), \quad (42b)$$

$$\boldsymbol{q} = 2\boldsymbol{v}_0 - \boldsymbol{v}_p - \boldsymbol{v}_e, \quad (42c)$$

and using Eq. (41b) with $\boldsymbol{c}=\boldsymbol{\kappa}$

$$\bar{v}^{+} = \mathrm{Max}(|2\boldsymbol{v}_0 - \boldsymbol{v}_e|, v_p), \quad (42d)$$

$$\bar{v}^{-} = \mathrm{Max}(|2\boldsymbol{v}_0 - \boldsymbol{v}_p|, v_e). \quad (42e)$$

Formulas (42a)–(42e) define the impulse approximation (IA) used in this paper. The TDCS is calculated from Eq. (22) by replacing f^{B1} by $f^{IA,\mathrm{Peak}}$ of Eq. (42a). Finally, we note that the peaking approximation described above has been used successfully in atom/ion collisions [5,6].

IV. CALCULATIONAL DETAILS

We consider fragmentation of Ps(1s) in collision with ground state He, Ne, Ar, Kr, and Xe. We have calculated f^{+}_{el} and f^{-}_{el} in the static and static exchange approximations in which the atom is frozen in its ground state. The atomic wave functions have been taken from Clementi and Roetti [29]. The static-exchange approximation for electon scattering allows for electron exchange between the Ps and the atom. In physical content, therefore, our calculations are the

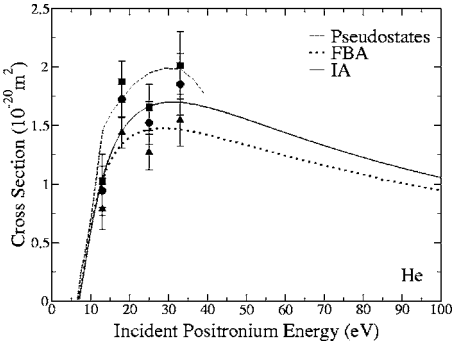

FIG. 2. Total cross sections for ionization of Ps in Ps($1s$) -He(1^1S) collisions. Theoretical curves correspond to target elastic ionization. Experimental data are from Refs. [11,12].

same as the frozen target coupled pseudostate approximations used by Blackwood *et al.* [14,18]. The form factors appearing in Eq. (42a) are easily evaluated analytically using results given in Appendix 2 of Ref. [3] which have been derived using the Nordsieck integration technique [30]. The lower order cross sections (DDCS, SDCS, etc.) have been evaluated from the TDCS by numerical integration. Here care must be taken in going from the TDCS to the DDCS on account of the infinite ELC cusp when $\boldsymbol{v}_p \rightarrow \boldsymbol{v}_e$. Thus, for example, in calculating $d^2\sigma_{bb'}/dEd\Omega_e$ one has to integrate the TDCS over

$$d\Omega_p = \sin\theta_p d\theta_p d\phi_p. \tag{43}$$

If the z axis is oriented along the direction of $\boldsymbol{v}_e$ then the $1/\kappa$ ELC singularity becomes, see Eq. (16),

$$\frac{2}{\sqrt{v_p^2 + v_e^2 - 2v_p v_e \cos\theta_p}}, \tag{44}$$

which is manifestly integrable as $\boldsymbol{v}_p \rightarrow \boldsymbol{v}_e$.

V. RESULTS

A. Total ionization cross section

Figure 2 compares calculated target elastic total ionization cross sections for Ps($1s$)-He(^1S) scattering [31] with the experimental data from Refs. [11,12]. We note that only target elastic ionization of the Ps is possible up to E_0=27 eV. The contribution of target inelastic ionization of Ps to the experimental data at E_0=33 eV is thought to be neglegible [14]. The calculated cross sections shown are the present IA and FBA results and the coupled pseudostates numbers of Blackwood *et al.* [14,32], the pseudostate numbers should be the most reliable. All the calculations are consistent with experiment and the FBA is suprisingly good at such low energies. This contrasts with the CTMC results of Sarkadi [16] which overestimate the experimental data by a factor of up to 2.5. The IA shows good convergence to the FBA results at energies beyond those shown in Fig. 2, the two are in agreement within 5% (1%) beyond about 175 eV (300 eV).

Figure 3 shows the target elastic total ionization cross sections for Ne, Ar, Kr, and Xe. For Ne and Ar we have the coupled pseudostate results of Blackwood *et al.* [18,32] for

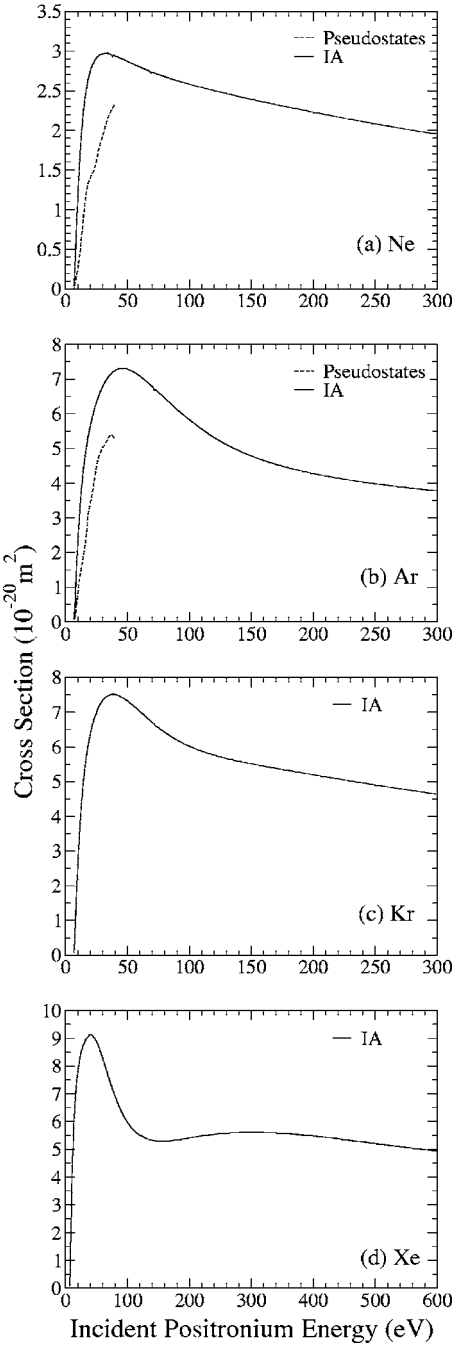

FIG. 3. Target elastic total ionization cross sections of Ps($1s$) in collision with (a) Ne, (b) Ar, (c) Kr, and (d) Xe. Solid curve, IA and dashed curve, coupled pseudostate results of Blackwood *et al.* [18].

comparison. Unlike Fig. 2, Figs. 3(a) and 3(b) show that the IA overestimates the pseudostate numbers in their given energy range of 0 to 40 eV. We would hope to see convergence of the two approximations at higher energies. The pseudostate numbers are to be regarded as the more reliable and on this basis Figs. 3(a) and 3(b) give us some feeling for the accuracy of the IA in the low energy region for the heavier targets. The IA result for Xe, Fig. 3(d) is interesting in that it shows a double maximum structure, a pronounced maximum at 41 eV, and a very broad maximum centered near 300 eV.

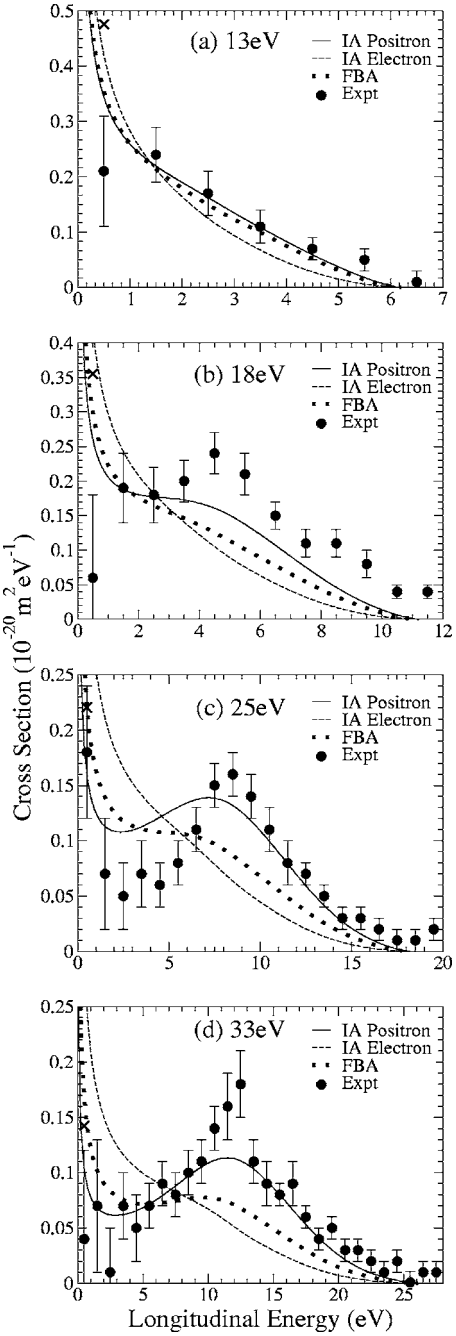

FIG. 4. Cross sections differential in longitudinal energy for Ps($1s$)+He(1^1S) collisions. Solid curve, IA SDCSLP; dashed curve, IA SDCSLE; and dotted curve, FBA. Experimental measurements of SDCSLP are from [11,12]. The cross gives the average value of the IA SDCSLP over the first bin from 0 to 1 eV.

B. Cross section differential in the longitudinal energy of the ejected positron or electron (SDCSLP and SDCSLE)

Figure 4 compares our target elastic IA results for SDCSLP with the experimental data for He [11,12]. The experimental points have been measured in 1 eV bins [11,19] and represent averages over the intervals 0 to 1 eV, 1 to 2 eV, etc. In Fig. 4 the experimental points have been placed at the centers of the bins, i.e., at 0.5 eV, 1.5 eV, etc. There is quite

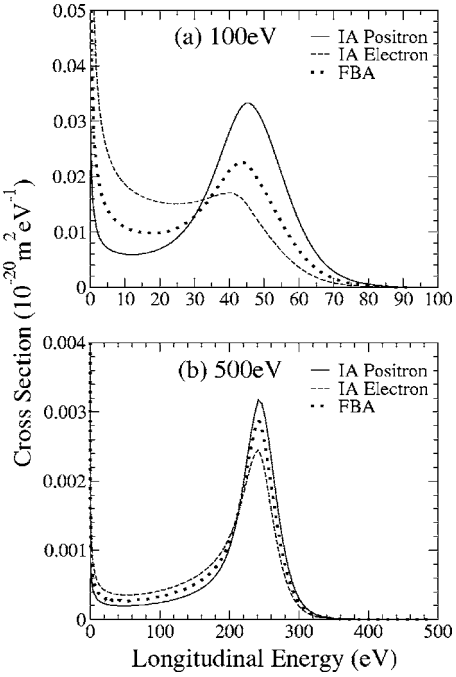

FIG. 5. Same as for Fig. 4.

good agreement between the IA and experiment on both shape and normalization. The CTMC calculation of Sarkadi [16] perhaps agrees marginally better with experiment on shape but fails totally on normalization. As shown in Sec. II, SDCSLP must diverge as $1/\sqrt{E_{pl}}$ as $E_{pl}\rightarrow 0$. The experimental points at 0.5 eV represent the average of this divergent cross section over the bin 0 to 1 eV. We have calculated this average and compare it with the experiment in Fig. 4. Except at $E_0=25$ eV, the agreement for this first bin is not so good.

Also shown in Fig. 4 are the target elastic IA results for the corresponding electron cross section, SDCSLE. Like Sarkadi [16] we find that SDCSLE is much slower than SDCSLP to develop a maximum with increasing impact energy, see Figs. 4 and 5, and that SDCSLE is larger than SDCSLP at small values of the longitudinal energy but becomes smaller with increasing longitudinal energy. Also shown in Figs. 4 and 5 is the target elastic FBA cross section which is the same for both positrons and electrons (Sec. III A). As one might guess, the FBA tends to be somewhere between the IA results for SDCSLP and SDCSLE.

Figure 5 shows the longitudinal cross sections at the much higher impact energies of 100 and 500 eV. At 100 eV there is still a substantial difference between the IA cross sections SDCSLP and SDCSLE with the electron cross section only just beginning to show a maximum. At 500 eV we see the two IA cross sections converging towards each other and sandwiching the FBA between them, now there is a very clear maximum in all three cross sections.

Figure 6 shows the target elastic IA results for SDCSLP and SDCSLE for Ps($1s$)+Xe collisions. With some interesting exceptions, that we now describe, the pattern is similar to that for He shown in Figs. 4 and 5 except that the scale of the cross sections is larger, by a factor of 5 at $E_0=33$, 50, and 100 eV, rising to a factor of 20 at $E_0=500$ eV. A noticeable difference from He is that SDCSLE acquires a maximum

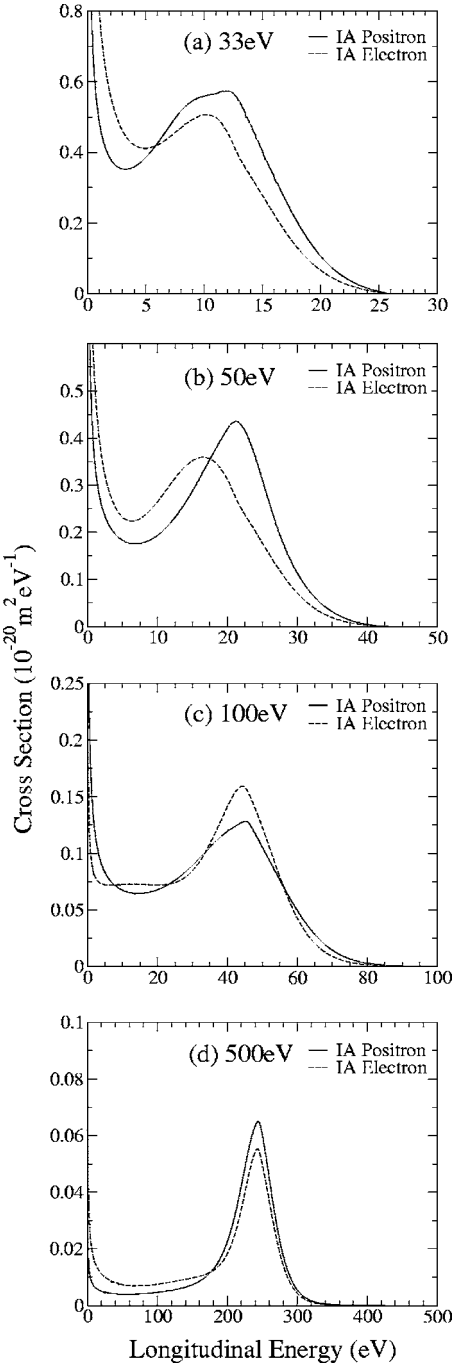

FIG. 6. Target elastic cross sections differential in the longitudinal energy for Ps($1s$)+Xe collisions, notation as in Fig. 4.

with increasing impact energy much more quickly, such a maximum already appears at $E_0=33$ eV while for He it does not appear until almost $E_0=100$ eV. The other interesting difference is a switch in the behaviors of SDCSLP and SDCSLE in the vicinity of $E_0=100$ eV, Fig. 6(c). At the other impact energies shown in Fig. 6, and as for He in Figs. 4 and 5, SDCSLE always lies above SDCSLP at low longitudinal energies and below SDCSLP where the latter displays its maximum, the reverse is true in Fig. 6(c); the normal pattern is restored by $E_0=500$ eV, Fig. 6(d). This switch in behaviors appears to be correlated with the dip near

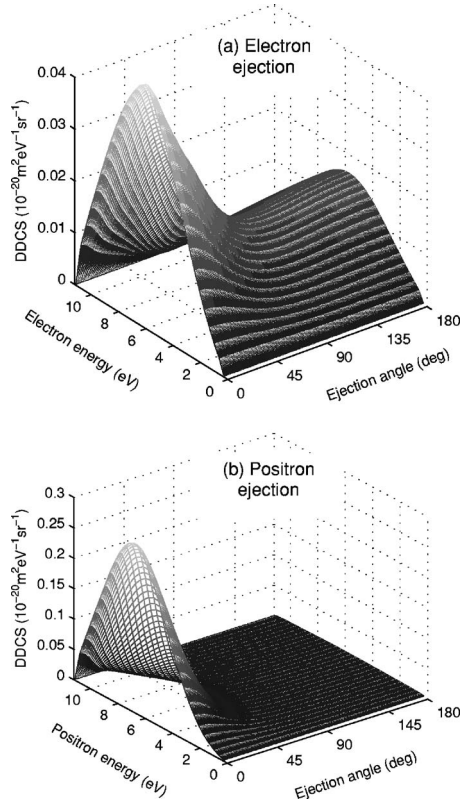

FIG. 7. Target elastic IA DDCSs for Ps($1s$) scattering by He(1^1S) at $E_0=18$ eV: (a) $d^2\sigma/dEd\Omega_e$ and (b) $d^2\sigma/dEd\Omega_p$.

$E_0=100$ eV in the total ionization cross section for Xe shown in Fig. 3(d).

C. Double differential cross sections

In Fig. 7 we show the target elastic IA cross sections $d^2\sigma/dEd\Omega_p$ and $d^2\sigma/dEd\Omega_e$ [33] for He at an impact energy of 18 eV. These should be compared with the CTMC results of Sarkadi [16] at the same impact energy. From Fig. 7 we see that $d^2\sigma/dEd\Omega_e$ is biggest for forward electron ejection. This is opposite to Sarkadi's prediction that backward electron ejection dominates, substantially. By contrast, the IA results for $d^2\sigma/dEd\Omega_p$ are more comparable in shape to Sarkadi's cross section. Figure 7 shows that, at the peak, $d^2\sigma/dEd\Omega_p$ is a factor of six larger than $d^2\sigma/dEd\Omega_e$. It is also seen that $d^2\sigma/dEd\Omega_e$ declines more slowly with increasing ejection angle than $d^2\sigma/dEd\Omega_p$ [34] and even shows a rise towards 180°, i.e., there is a backward peak, but not the dominant backward peak seen by Sarkadi.

Sarkadi [16] has put forward a possible explanation for the large backward peak in his calculation of $d^2\sigma/dEd\Omega_e$. The argument goes as follows. At low energies, e.g., 18 eV, the collision is adiabatic. The Ps then becomes polarized, the electron being attracted by the static field of the He atom, the positron being repelled. As a consequence, the electron is, on average, closer to the target nucleus than the positron. The probability that the electron undergoes a hard collision with the atom is then increased, resulting in a large angle deflection of the electron. This hypothesis remains to be verified.

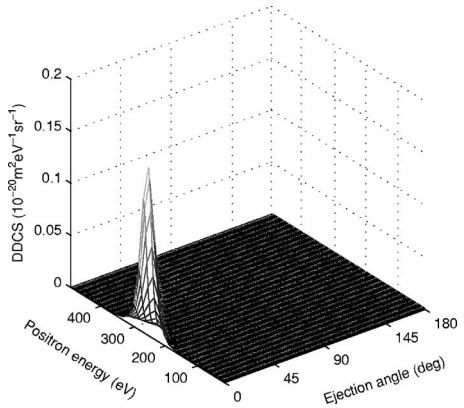

FIG. 8. Target elastic IA DDCS $d^2\sigma/dEd\Omega_p$ for Ps($1s$) scattering by He(1^1S) at $E_0=500$ eV.

Certainly, such a polarization mechanism is absent from our IA. Thus the IA (42a) may be interpreted as involving the collision of the positron or electron with the atom, represented by the scattering amplitude $f_{el}^{\pm}$, while the remaining electron or positron is shaken off, represented by the form factor term. Clearly, there is no role for polarization of the Ps in this interpretation. If the hypothesis of Sarkadi is correct, then it could explain the absence of the large backward scattering in our $d^2\sigma/dEd\Omega_e$. By contrast, the Sarkadi hypothesis implies a soft collision of the positron with the atom resulting in a forwardly peaked $d^2\sigma/dEd\Omega_p$, consistent both with his result and ours. Another possibility is that the inclusion of electron exchange in our IA model has changed the picture, recall that Sarkadi [16] ignores exchange effects. We have recalculated $d^2\sigma/dEd\Omega_e$ switching off electron exchange between the Ps and the He atom, i.e., using only the static approximation to calculate f_{el}^{-}. The picture remains very similar to Fig. 7, i.e., exchange is not the cause of the difference between Sarkadi and us.

Figure 8 shows $d^2\sigma/dEd\Omega_p$ for He at an impact energy of 500 eV. The result for $d^2\sigma/dEd\Omega_e$ is similar but a factor of 2 smaller at the peak. Figure 8 displays a sharply peaked cross section centered near 246.6 eV and $\theta_p=0°$, indicating that the electron and positron tend to be ejected in the forward direction with nearly equal energies. This statement is also consistent with Fig. 7 and all the cases we have looked at from $E_0=13$ eV upwards.

With two qualifications the IA DDCS results for Xe are similar to He but larger in scale. The first qualification concerns the relative peak heights of $d^2\sigma/dEd\Omega_e$ and $d^2\sigma/dEd\Omega_p$. These are in agreement with the pattern for He, i.e., $d^2\sigma/dEd\Omega_e$ gives a noticeably smaller peak, except in a transitional region around 100 eV. Here we find that $d^2\sigma/dEd\Omega_e$ can have the larger peak. This transitional region was also observed in Fig. 6 for the longitudinal cross sections where a switch in the patterns of positron and electron ejection was seen at $E_0=100$ eV, Fig. 6(c). Like Fig. 6, the normal pattern of behavior resumes on going to still higher impact energies.

The second qualification concerns the large angle behavior of $d^2\sigma/dEd\Omega_e$. This is illustrated in Fig. 9(a) for an

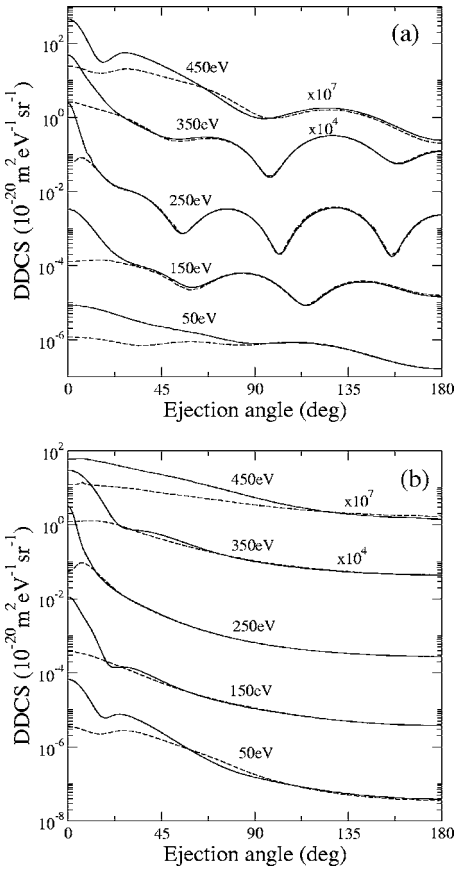

FIG. 9. Target elastic IA DDCSs for Ps($1s$) scattering by ground state Xe at $E_0=500$ eV: (a) $d^2\sigma/dEd\Omega_e$ and (b) $d^2\sigma/dEd\Omega_p$. The energy of the ejected electron, E_e, is indicated on each curve; the corresponding energy of the ejected positron is $E_p=(E_0-6.8-E_e)$eV. Solid curve: full calculation using Eqs. (42a)–(42e). Dashed curve: in (a) calculated with f_{el}^{+} set to zero in Eq. (42a), and in (b) calculated with f_{el}^{-} set to zero in Eq. (42a).

impact energy of 500 eV. Here we observe a pronounced dip-bump structure for an electron ejection energy, E_e, of 250 eV. This structure fades as E_e moves away from equal energy sharing between the electron and the positron. Referring to Fig. 1, we note the striking resemblance of the $E_e=250$ eV curve to the differential cross section for free electron scattering at 250 eV. Also shown in Fig. 9(a) is $d^2\sigma/dEd\Omega_e$ calculated by setting f_{el}^{+} to zero in Eq. (42a), i.e., only electron scattering contributes. This cross section comes into good agreement with the full calculation as the ejection angle increases, the agreement being particularly good at $E_e=250$ eV. This decisively confirms the identification of the dip-bump structure with that seen in the free electron scattering of Fig. 1 and is consistent with the physical picture that larger deflections of the electron require a collision between the electron and the atom rather than a shake-off after the positron has collided, as represented by the first term in Eq. (42a). The situation for $d^2\sigma/dEd\Omega_p$ is analogous, as shown in Fig. 9(b). Here we see a smooth cross section for $E_e=250$ eV, like in the free positron scattering of Fig. 1, but now with structure creeping in as E_e moves away from equal

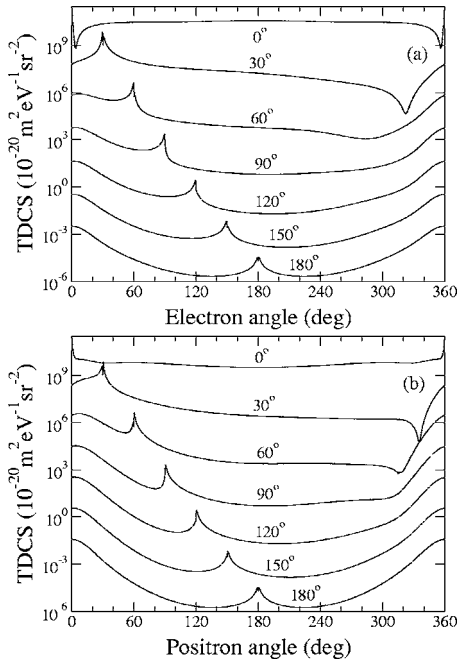

FIG. 10. TDCS in coplanar geometry for Ps($1s$) incident upon He(1^1S)) at 33 eV; the ejected positron and electron have energies of 13 and 13.2 eV, respectively. (a) Shows the TDCS as a function of the electron angle θ_e for fixed positron angles θ_p; in (b) θ_e is fixed and θ_p is varied. The fixed angle is indicated on each curve. The curves have been staggered by a factor of 10^2 on decreasing the fixed angle from 180°.

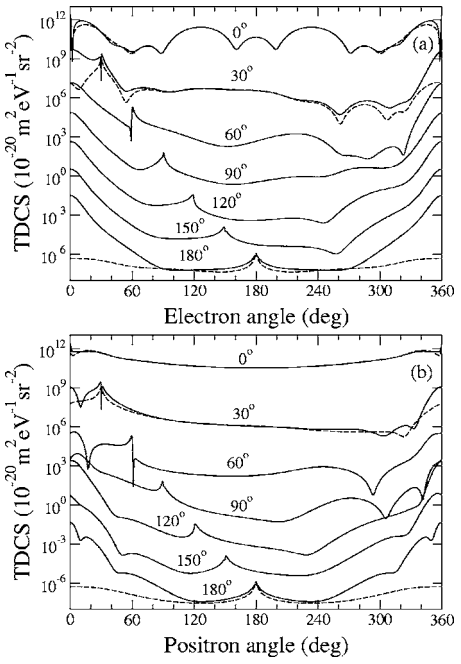

FIG. 11. As in Fig. 10 but for Ps($1s$) incident upon ground state Xe at 100 eV. The ejected positron and electron have energies of 46 and 47.2 eV, respectively. Solid curve, full calculation using Eqs. (42a)–(42e). Dashed curve (shown only for 0°, 30°, and 180°): in (a) calculated with f_{el}^{+} set to zero in Eq. (42a), and in (b) calculated with f_{el}^{-} set to zero in Eq. (42a).

energy sharing. By setting f_{el}^{-} equal to zero in Eq. (42a) we see that the large angle cross section in Fig. 9(b) comes essentially from the positron scattering term. Figure 9 demonstrates that, where free positron and free electron scattering by an atom are sufficiently different in form, it should be possible to observe the difference in the DDCSs.

D. Triple differential cross sections

In Figs. 10 and 11 we show examples of the TDCS for He and Xe at impact energies of 33 and 100 eV, respectively. In both cases the geometry is coplanar, i.e., the vectors $\boldsymbol{v}_0, \boldsymbol{v}_p$, and $\boldsymbol{v}_e$ all lie in the same plane. The cross sections are given as a function of θ_e for fixed θ_p, or vice versa, where $\theta_e(\theta_p)$ is the angle which the ejected electron (positron) makes with the incident direction. Note that our convention is $0° \leqslant \theta_p, \theta_e \leqslant 360°$. The cases shown correspond to almost equal energy sharing between the ejected particles, consequently, in all curves we observe an ELC cusp (Sec. III A) whenever $\theta_e = \theta_p$. Interestingly, however, we see that in some cases the cusps have structure. This structure derives from a subtle interplay between the two terms in Eq. (42a) and depends upon both the behavior of the form factors and the free scattering amplitudes $f_{el}^{\pm}$. These structures are not present in all cusps nor at all impact energies.

The smoothness of the $\theta_p = 0°$ TDCS for He as a function of the electron angle θ_e, Fig. 10(a), contrasts with the pronounced structure in the corresponding cross section for Xe, Fig. 11(a). This reflects the contrast between the smooth differential cross sections for free electron scattering by He (not shown here) and the structured cross sections for Xe illustrated in Fig. 1. As in Fig. 9, this is demonstrated by the dashed cross section in Fig. 11(a) which is the result obtained by setting f_{el}^{+} to zero in Eq. (42a). Here we observe that at $\theta_p = 0°$ and 30° there is very good agreement with the full IA calculation when the electron is ejected at large angles relative to the forward direction [35], i.e., once more (see Sec. V C) we see that large angle ejection of the electron requires the electron to be scattered by the target [the second term in Eq. (42a)] and not just shaken off [the first term in Eq. (42a)]. The situation for positron ejection is analogus, Fig. 11(b). We also note from Fig. 11 that, unlike the solid curves, the cusps in the dashed curves have no structures, this illustrates that the structures in the cusps come from the interplay between the two terms in Eq. (42a).

VI. CONCLUSIONS

Our results confirm the general predictions of the CTMC calculations of Sarkadi [16] for the Ps($1s$)+He(1^1S) system but differ on detail. Thus we support the predicted relative behavior of the longitudinal cross sections for positron and electron ejection (SDCSLP and SDCSLE) but we get much better agreement with experiment on the absolute size of the longitudinal positron cross section (SDCSLP) and of the total Ps ionization cross section.

Unlike CTMC, our calculations are fully quantal and allow for electron exchange between the Ps and the atom. Like CTMC, we do not take account of the possibility of excitation or ionization of the atom. For comparison with existing experimental data on He that is adequate, since the impact energies are relatively low ($\leqslant$33 eV), but with rising impact energy excitation or ionization of the target becomes increasingly important and usually dominant [13]. We shall treat this somewhat different situation in another publication.

We have gone beyond the study of Sarkadi [16], looking at higher impact energies and much heavier targets such as Xe, and examining the most fundamental cross section of all, the triple differential cross section (TDCS). The heavier targets are interesting because of the structures they inherit, primarily from the interaction of the Ps electron with the target. We have seen that, where the patterns of free electron and free positron scattering by the target are sufficiently different, it is possible to distinguish these differences not only in the TDCS but also in the double differential cross sections. Of course, the difference in patterns is possibly not as clear as our static and static-exchange approximations of Fig. 1 would have us believe, but, where there is sufficient difference, it should be observable in Ps scattering at the double and triple differential levels. Experiments on the heavier targets are to be encouraged.

Some comments on our approximation are in order. We have used the impulse approximation (IA) but a form modified by a peaking approximation. For ionization this peaking assumption is probably quite good, certainly calculations using this version of the IA have worked reasonably well for ionization of heavy particles [4,5]. The IA is in essence a "high energy" approximation. Roughly speaking, the greater the ratio of the impact energy to the binding energy of the projectile the better the approximation should be. Thus the approximation would be expected to work better for Ps($2s$) than Ps($1s$). The approximation requires free electron-target and free positron-target scattering amplitudes as input. These are needed over a range of energies and scattering angles. We have used the static-exchange and static approximations, respectively, for this purpose. In particular, the static-exchange approximation allows for electron exchange between the Ps and the atom. While it would be nice to see how better approximations perform, we believe that the static-exchange and static approximations are adequate for present purposes.

ACKNOWLEDGMENTS

We are grateful to Professor G. Laricchia for providing us with the data from Refs. [11,12] and for information on the experiment. This work was supported by EPSRC grants GR/N07424, GR/R83118/01, and GR/R62557/01 and by the Department for Employment and Learning Northern Ireland (DEL).

APPENDIX A: FORMULA FOR TDCS

In this appendix we derive the basic formula used in Eq. (22) for the TDCS in terms of the scattering amplitude. Without approximation the scattering amplitude for Ps ionization may be written

$$f^{free} = -\frac{1}{(2\pi)^{5/2}} \int e^{-i\boldsymbol{v}_p\cdot\boldsymbol{r}_p} e^{-i\boldsymbol{v}_e\cdot\boldsymbol{r}_e} \psi^*_{b'}(\boldsymbol{X}) \times (V + V_{Ps})\Psi^+ d\boldsymbol{r}_p d\boldsymbol{r}_e d\boldsymbol{X}, \tag{A1}$$

where Ψ^+ is the exact wave function for the system,

$$\Psi^+ \overset{R\to\infty}{\longrightarrow} e^{i\boldsymbol{p}_0\cdot\boldsymbol{R}}\phi_a(\boldsymbol{t})\psi_b(\boldsymbol{X}) + \text{outgoing scattered waves}. \tag{A2}$$

V, defined in Eq. (12), is the interaction of the atom with the Ps electron and positron,

$$V_{\mathrm{Ps}} = -\frac{1}{|\boldsymbol{r}_p - \boldsymbol{r}_e|} \tag{A3}$$

is the interaction between the Ps electron and positron, and the asterisk denotes complex conjugation. In Eq. (A1) we think of the Coulomb potential as a finite range potential of arbitrarily long range, this is possible to all practical intents and purposes. Outside the range of the Coulomb interaction the ejected positron and electron move freely and can be represented by the plane waves $e^{i\boldsymbol{v}_p\cdot\boldsymbol{r}_p}$ and $e^{i\boldsymbol{v}_e\cdot\boldsymbol{r}_e}$. With the normalization (A1) the TDCS is then given by [20,21]

$$\frac{d^3\sigma_{bb'}}{dEd\Omega_e d\Omega_p} = \frac{v_p v_e}{v_0}|f^{free}|^2. \tag{A4}$$

Following Curran [20] and Whelan *et al.* [21] we can use the two-potential formula [22] to absorb the interaction (A3) into the final state of the electron and positron which now becomes a continuum state $\phi^-_{\boldsymbol{\kappa}}$ of Ps [as defined in Eq. (17)] whose center of mass moves with velocity $\boldsymbol{v}_f = \frac{1}{2}(\boldsymbol{v}_p + \boldsymbol{v}_e)$, i.e.,

$$\frac{1}{(2\pi)^{3/2}} e^{i\boldsymbol{v}_p\cdot\boldsymbol{r}_p} e^{i\boldsymbol{v}_e\cdot\boldsymbol{r}_e} \rightarrow \phi^-_{\boldsymbol{\kappa}}(\boldsymbol{t}) e^{i\boldsymbol{p}_f\cdot\boldsymbol{R}}, \tag{A5}$$

where $\boldsymbol{p}_f = 2\boldsymbol{v}_f = \boldsymbol{v}_p + \boldsymbol{v}_e$. Changing the variables of integration in Eq. (A1) according to

$$d\boldsymbol{r}_p d\boldsymbol{r}_e d\boldsymbol{X} = d\boldsymbol{R} d\boldsymbol{t} d\boldsymbol{X} \tag{A6}$$

the amplitude (A1) becomes

$$f^{free} = \frac{1}{2}\left(-\frac{1}{\pi} \int e^{-i\boldsymbol{p}_f\cdot\boldsymbol{R}} \phi^{-*}_{\boldsymbol{\kappa}}(\boldsymbol{t}) \psi^*_{b'} V \Psi^+ d\boldsymbol{R} d\boldsymbol{t} d\boldsymbol{X} \right). \tag{A7}$$

The term is brackets is the amplitude, f^{Ps} say, that we would naturally write down if we thought of the final state of the electron and positron as being a state of Ps, as we do in Eq. (11). In terms of f^{Ps} the TDCS is then

$$\frac{d^3\sigma}{dEd\Omega_e d\Omega_p} = \frac{v_p v_e}{4v_0}|f^{Ps}|^2 \tag{A8}$$

which explains formula (22).

APPENDIX B: ASYMPTOTIC IMPACT ENERGY DEPENDENCE OF THE TOTAL IONIZATION CROSS SECTION

At asymptotic energies the FBA applies and from Eq. (3)

$$\sigma_{bb'}^{ion} = \int \frac{d^3\sigma_{bb'}^{B1}}{dE d\Omega_e d\Omega_p} dE d\Omega_e d\Omega_p. \tag{B1}$$

However, for present purposes, formula (19) gives a better starting point,

$$\sigma_{bb'}^{ion} = \int \frac{d^3\sigma_{bb'}^{B1}}{d\Omega_{\rm Ps} d\boldsymbol{\kappa}} d\Omega_{\rm Ps} \kappa^2 d\kappa d\Omega_\kappa, \tag{B2}$$

since the first Born amplitude (20) is explicitly a function of $\boldsymbol{\kappa}$ and $\boldsymbol{q}$ (in fact a function of κ, q and $\boldsymbol{\kappa}\cdot\boldsymbol{q}$ if the states ϕ_a, ψ_b, and $\psi_{b'}$ are spherically symmetric). From $\boldsymbol{q}=\boldsymbol{p}_0-\boldsymbol{p}_f$ we can write

$$d\Omega_{\rm Ps} = \frac{q dq}{p_0 p_f} d\phi_q \tag{B3}$$

where ϕ_q is the azimuthal angle of $\boldsymbol{q}$ about $\boldsymbol{p}_0$ as z direction. In the limit $E_0 \to \infty$ the leading behavior of Eq. (B2) is therefore given by

$$\sigma_{bb'}^{ion} = \frac{1}{4E_0} \int_0^\infty q dq \int_0^{2\pi} d\phi_q \int_0^\infty \kappa^2 d\kappa \times \int_{-1}^1 d(\cos\theta_\kappa) \int_0^{2\pi} d\phi_\kappa \times |f^{B1}(\mathrm{Ps}{:}a \to \boldsymbol{\kappa}; \mathrm{atom}{:}b \to b')|^2. \tag{B4}$$

We note that as $q \to 0$ the amplitudes $f_{bb'}^{B1\pm}(\boldsymbol{q})$ in Eq. (20) behave at worst as $1/q$ [see Eq. (14)], while the form factors $\langle \phi_{\boldsymbol{\kappa}}^-(\boldsymbol{t}) | e^{\pm i\boldsymbol{q}\cdot\boldsymbol{t}/2} | \phi_a(\boldsymbol{t}) \rangle$ tend to zero at least as fast as q, thus f^{B1} is finite in this limit. As $\kappa \to 0$ the $1/\kappa$ singularity in $|f^{B1}|^2$, see Eq. (23), is killed by the κ^2 in Eq. (B4). There are no other singularities in $|f^{B1}|^2$. As q and κ tend to ∞, $|f^{B1}|^2$ dies off sufficiently rapidly for the integrals in Eq. (B4) to be convergent. Consequently, in the limit $E_0 \to \infty$ the leading behavior of $\sigma_{bb'}^{ion}$ is $1/E_0$, i.e., there is no $\ln E_0/E_0$ term as one gets for ionization by charged particles.

[1] J. Ludlow and H. R. J. Walters, in *Many-Particle Spectroscopy of Atoms, Molecules, Clusters, and Surfaces*, edited by J. Berakdar and J. Kirschner (Kluwer/Plenum, New York, 2001), p. 319.
[2] G. F. Chew, Phys. Rev. **50**, 196 (1950).
[3] J. P. Coleman, in *Case Studies in Atomic Physics I*, edited by E. W. McDaniel and M. R. C. McDowell (North-Holland, Amsterdam, 1969), p. 101.
[4] H. M. Hartley, thesis, The Queen's University of Belfast, 1981.
[5] H. M. Hartley and H. R. J. Walters, J. Phys. B **20**, 3811 (1987).
[6] H. M. Hartley and H. R. J. Walters, J. Phys. B **21**, L43 (1988).
[7] N. Zafar, G. Laricchia, M. Charlton, and A. J. Garner, Phys. Rev. Lett. **76**, 1595 (1996).
[8] A. J. Garner, A. Özen, and G. Laricchia, Nucl. Instrum. Methods Phys. Res. B **143**, 155 (1998).
[9] A. J. Garner, A. Özen, and G. Laricchia, J. Phys. B **33**, 1149 (2000).
[10] S. Armitage and G. Laricchia, Nucl. Instrum. Methods Phys. Res. B **192**, 67 (2002).
[11] S. Armitage, D. E. Leslie, A. J. Garner, and G. Laricchia, Phys. Rev. Lett. **89**, 173402 (2002).
[12] G. Laricchia, S. Armitage, and D. E. Leslie, Nucl. Instrum. Methods Phys. Res. B **221**, 60 (2004).
[13] M. T. McAlinden, F. G. R. S. MacDonald, and H. R. J. Walters, Can. J. Phys. **74**, 434 (1996).
[14] J. E. Blackwood, C. P. Campbell, M. T. McAlinden, and H. R. J. Walters, Phys. Rev. A **60**, 4454 (1999).
[15] From here on we shall use the term "excited" to mean either discrete excitation or ionization.
[16] L. Sarkadi, Phys. Rev. A **68**, 032706 (2003).
[17] H. M. Hartley and H. R. J. Walters, J. Phys. B **20**, 1983 (1987).
[18] J. E. Blackwood, M. T. McAlinden, and H. R. J. Walters, J. Phys. B **35**, 2661 (2002); **36**, 797 (2003).
[19] G. Laricchia (private communication).
[20] E. P. Curran, thesis, The Queen's University of Belfast, 1986.
[21] C. T. Whelan, H. R. J. Walters, and X. Zhang, in $(e,2e)$ *and Related Processes*, edited by C. T. Whelan, H. R. J. Walters, A. Lahmam-Bennani, and H. Ehrhardt (Kluwer, Dordrecht, 1993), p. 1.
[22] M. L. Goldberger and K. M. Watson, *Collision Theory* (Wiley, New York, 1964), pp. 202–209.
[23] M. Abramowitz and I. A. Stegun, *Handbook of Mathematical Functions*, (Dover, New York, 1965).
[24] F. Drepper and J. S. Briggs J. Phys. B **9**, 2063 (1976); **11**, 4033 (1978).
[25] H. R. J. Walters, J. Phys. B **8**, L54 (1975).
[26] D. P. Dewangan and H. R. J. Walters, J. Phys. B **11**, 3983 (1978).
[27] Reference [22], p. 79.
[28] For example, if we switch off the Coulomb interaction between the electron and the positron the $\phi_{\boldsymbol{\kappa}}^-$ becomes a plane wave state and $g_{a'}(\mathbf{Q}'')$ will be a pure delta function centered at $\mathbf{Q}''=\boldsymbol{\kappa}$.
[29] E. Clementi and C. Roetti, At. Data Nucl. Data Tables **14**, 177 (1974).
[30] A. Nordsieck, Phys. Rev. **93**, 785 (1954).
[31] It matters not whether the projectile is o-Ps$(1s)$ or p-Ps$(1s)$ or whether it is spin polarized, the results are the same. Accordingly, we refer to the projectile as simply Ps$(1s)$.

[32] Some small scale pseudostructure has been smoothed out of the pseudostate cross sections of Blackwood *et al.* [14,18] which was not apparent on the logarithmic scale used by Blackwood *et al.*

[33] The theoretical cross sections are only for target elastic collisions. In the interest of simplicity we drop the "*bb*" subscript that should be on the σ, where ψ_b is the ground state of the atom.

[34] This is not supprising since the integrals of $d^2\sigma/dEd\Omega_e$ and $d^2\sigma/dEd\Omega_p$ over $d\Omega_e$ and $d\Omega_p$, respectively, have to be equal.

[35] Note that both $\theta=0°$ and $\theta=360°$ correspond to the forward direction.